PERGAMON

International Journal of Solids and Structures 38 (2001) 5949–5962

INTERNATIONAL JOURNAL OF SOLIDS and STRUCTURES

www.elsevier.com/locate/ijsolstr

# Development of a three-dimensional mixed variational model for woven composites. II. Numerical solution and validation

Sangwook Sihn [a], Ajit K. Roy [b,*]

[a] *University of Dayton Research Institute, 300 College Park Ave., Dayton, OH 45469-0168, USA*

[b] *Air Force Research Laboratory, Materials and Manufacturing Directorate, AFRL/MLBC, 2941 P St Rm. 136, WPAFB, OH 45433-7750, USA*

Received 23 March 2000

**Abstract**

A mixed three-dimensional variational model, derived in an adjoining paper, is solved numerically for stress analysis with a finite element approach. Since the mixed model calculates the stress field by taking variations of displacement and stresses independently and satisfying equilibrium of stresses pointwise, accurate interlaminar stresses are predicted at the yarn interface. The interface continuity conditions are implemented through a penalty method by adding an additional variational energy of two constraint conditions: the displacements must be continuous along the interface between two stacked subregions, and interfacial normal and shear stresses must be in equilibrium at the interface. After performing the thickness integration, the three-dimensional variational energy equation is evaluated for each yarn (subregion) two-dimensionally with 16 stress-related and 13 displacement-related unknown variables. Rayleigh–Ritz approximation yields a system of linear equations by taking derivatives of the variational energy equation with respect to the independent unknown variables. The present mixed method is applied to analyze a flat laminated composite with a free edge, and the representative volume element of woven fabric composites. The displacement and stress results of the present method are compared and validated with the conventional displacement-based finite element solutions and/or the previous analytic solution. 

*Keywords:* Reissner variational principle; Penalty method; Rayleigh–Ritz approximation; Free-edge problem; Woven fabric composite

## 1. Introduction

To obtain reliable interlaminar stresses at the interface in an efficient manner, a three-dimensional analytical model has been proposed based on Reissner's variational principle (Reissner, 1950; Pagano, 1978; Harrison and Johnson, 1996). The model takes independent variations on the stress and the displacement components. This mixed variational principle yields a variational energy in the form of the stresses as well as the displacements. Since the mixed model calculates the stress field by taking variations of displacement

* Corresponding author. Tel.: +1-937-255-9034; fax: +1-937-656-4707.
*E-mail address:* ajit.roy@wpafb.af.mil (A.K. Roy).

0020-7683/01/$ - see front matter 
PII: S0020-7683(00)00405-4

and stresses independently and satisfying equilibrium of stresses pointwise, accurate interlaminar stresses are predicted at the yarn interface.

The derivation of the mixed three-dimensional variational model of a representative volume element (RVE) of woven fabric composites, based on the Reissner variational principle, is given in part I, an adjoining paper by Roy and Sihn (2000). In this model, an accurate prediction of the interlaminar stresses at the yarn (subregion) interface is achieved (except near the point of singularity) by satisfying the interface traction continuity conditions and the equilibrium of stresses pointwise. The in-plane stresses within a yarn are assumed to vary linearly in the thickness direction, and the expressions for the interlaminar stresses are obtained by satisfying the three-dimensional equilibrium equations. After performing the thickness integration, the three-dimensional variational energy equation is reduced to a two-dimensional equation and evaluated for each yarn (subregion) with 16 stress-related and 13 displacement-related unknown variables.

In this part of the present paper, a mixed finite element solution procedure is established based on the mixed variational principle, derived in part I of this work (Roy and Sihn, 2000). The total variational energy is obtained by accumulating the energy for all yarn and matrix subregions. The interface continuity conditions are implemented through a penalty method by adding an additional variational energy of two constraint conditions: the displacements must be continuous along the interface between two stacked subregions, and interfacial normal and shear stresses must be in equilibrium at the interface. Two large numbers of penalty parameters enforcing the displacement and stress continuity are employed carefully to avoid numerical errors.

The solution to the variational energy equation, derived in part I, is obtained by Rayleigh–Ritz approximation with polynomial shape functions. The present mixed solution technique is applied to analyze a flat laminated composite with a free edge, and the RVE of plain-weave woven composites. The displacement and stress results of the present method are compared and validated with the conventional displacement-based finite element solutions and/or the previous analytic solution.

## 2. Modified variational energy equation

The variational energy equation in Eq. (14) in part I is evaluated for a given ($k$th) subregion such as

$$
\begin{aligned}
J^{(k)} = & \int\int_{xy} [(\mu_{ij}+\chi_{ij})p_{ij} - (F_1\bar{u}+F_2u^*+F_3\bar{v}+F_4v^*+F_5\bar{w}+F_6w^*+F_7\hat{w})]^{(k)}\mathrm{d}x\,\mathrm{d}y \\
& + \int\int_{xy} [(p_{52}-h_{2,x}p_{12}-h_{2,y}p_{62})u_2 - (p_{51}-h_{1,x}p_{11}-h_{1,y}p_{61})u_1 + (p_{42}-h_{2,x}p_{62}-h_{2,y}p_{22})v_2 \\
& \qquad - (p_{41}-h_{1,x}p_{61}-h_{1,y}p_{21})v_1 + (p_{32}-h_{2,x}p_{52}-h_{2,y}p_{42})w_2 - (p_{31}-h_{1,x}p_{51}-h_{1,y}p_{41})w_1]^{(k)}\mathrm{d}x\,\mathrm{d}y \\
& + \int_x [(p_{61}\bar{u}+p_{62}u^*+p_{21}\bar{v}+p_{22}v^*+p_{41}\bar{w}+p_{42}w^*+p_{43}\hat{w})(h_2-h_1)]^{(k)}\Big|_{y_1}^{y_2}\mathrm{d}x \\
& + \int_y [(p_{11}\bar{u}+p_{12}u^*+p_{61}\bar{v}+p_{62}^{(k)}v^*+p_{51}\bar{w}+p_{52}w^*+p_{53}\hat{w})(h_2-h_1)]^{(k)}\Big|_{x_1}^{x_2}\mathrm{d}y \\
& - \int_\Gamma [(\tilde{\tau}_{x_2}u_2+\tilde{\tau}_{y_2}v_2+\tilde{\tau}_{z_2}w_2) - (\tilde{\tau}_{x_1}u_1+\tilde{\tau}_{y_1}v_1+\tilde{\tau}_{z_1}w_1)]^{(k)}\mathrm{d}\Gamma = 0
\end{aligned} \tag{1}
$$

where $\mu_{ij}$ and $\chi_{ij}$ are defined in Appendix A in part I (Roy and Sihn, 2000).

The interface continuity condition dictates that the displacements must be continuous along the interface between two stacked subregions ($k$th and $l$th subregions), and interfacial normal and shear stresses must be in equilibrium, as Fig. 1 shows.

By setting the interfacial normal stress as $\hat{\sigma}_3$ and interfacial shear stresses as $\hat{\sigma}_4$ and $\hat{\sigma}_5$, the interface continuity condition provides the following constraint conditions.

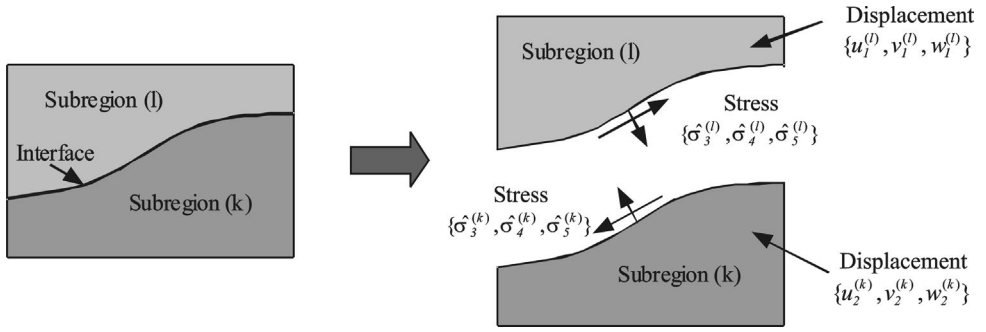


Fig. 1. Displacement and stress continuity at the interface between $k$th and $l$th subregions.

(1) Displacement continuity:

$$\begin{aligned} u_2^{(k)} - u_1^{(l)} &= 0 \\ v_2^{(k)} - v_1^{(l)} &= 0 \\ w_2^{(k)} - w_1^{(l)} &= 0 \end{aligned} \tag{2}$$

(2) Normal and shear stress continuity:

$$\begin{aligned} \hat{\sigma}_3^{(k)} - \hat{\sigma}_3^{(l)} &= 0 \\ \hat{\sigma}_4^{(k)} - \hat{\sigma}_4^{(l)} &= 0 \\ \hat{\sigma}_5^{(k)} - \hat{\sigma}_5^{(l)} &= 0 \end{aligned} \tag{3}$$

where $\hat{\sigma}_i^{(k)}$ and $\hat{\sigma}_i^{(l)}$ are the interfacial stress components at the $k$th and $l$th subregions, respectively. Note that the interfacial stresses are evaluated along the interfacial surfaces. These local stress components in the local $t$–$s$–$n$ coordinate system are related with the global stress components in the global $x$–$y$–$z$ coordinates by the slopes of the interfacial surfaces in $x$- and $y$-directions ($h_{2,x}^{(k)}$ and $h_{2,y}^{(k)}$), as shown in Fig. 4 and Table 1 in part I. Stress transformation using the direction cosines of the interfacial surface vectors yields the following stress constraint equations in the global coordinate system:

$$\begin{aligned} \hat{\sigma}_3^{(k)} - \hat{\sigma}_3^{(l)} = 0 &\Rightarrow \sigma_3^{(k)} - \sigma_3^{(l)} - h_{2,x}^{(k)}(\sigma_5^{(k)} - \sigma_5^{(l)}) - h_{2,y}^{(k)}(\sigma_4^{(k)} - \sigma_4^{(l)}) = 0 \\ \hat{\sigma}_4^{(k)} - \hat{\sigma}_4^{(l)} = 0 &\Rightarrow \sigma_4^{(k)} - \sigma_4^{(l)} - h_{2,x}^{(k)}(\sigma_6^{(k)} - \sigma_6^{(l)}) - h_{2,y}^{(k)}(\sigma_2^{(k)} - \sigma_2^{(l)}) = 0 \\ \hat{\sigma}_5^{(k)} - \hat{\sigma}_5^{(l)} = 0 &\Rightarrow \sigma_5^{(k)} - \sigma_5^{(l)} - h_{2,x}^{(k)}(\sigma_1^{(k)} - \sigma_1^{(l)}) - h_{2,y}^{(k)}(\sigma_6^{(k)} - \sigma_6^{(l)}) = 0 \end{aligned} \tag{4}$$

To impose the constraint conditions for displacement and stress continuity, one can substitute them into Eq. (1) directly to make an irreducible form. However, this method requires quite an involved algebraic manipulation. Even Eq. (17) in part I is not totally in an irreducible form, because $\chi_{ij}$ contains terms of all stress components. Moreover, when obtaining numerical solutions by polynomial shape functions, the restriction of excessive continuity for stresses should be avoided at singularities and at abrupt material property change interfaces. The imposition of such continuity is expected to produce erroneous (and usually highly oscillating) results (Zienkiewicz and Taylor, 1988).

Instead of the irreducible form, a penalty approach is introduced by adding a new energy term ($J_c$) for the constraint conditions in Eq. (2) in part I, with penalty parameters ($\alpha_1$ and $\alpha_2$), which yields a modified variational energy equation such as

$$\bar{J} = \sum_{k=1}^{M} J^{(k)} + \sum_{k=1}^{M-1} J_{\mathrm{c}}^{(k)} \tag{5}$$

where

$$\begin{aligned} J_{\mathrm{c}}^{(k)} = {} & \frac{1}{2}\alpha_1 \int\int_{xy} \left[ (u_2^{(k)} - u_1^{(l)})^2 + (v_2^{(k)} - v_1^{(l)})^2 + (w_2^{(k)} - w_1^{(l)})^2 \right] \mathrm{d}x\,\mathrm{d}y \\ & + \frac{1}{2}\alpha_2 \int\int_{xy} \left[ (\hat{\sigma}_3^{(k)} - \hat{\sigma}_3^{(l)})^2 + (\hat{\sigma}_4^{(k)} - \hat{\sigma}_4^{(l)})^2 + (\hat{\sigma}_5^{(k)} - \hat{\sigma}_5^{(l)})^2 \right] \mathrm{d}x\,\mathrm{d}y \end{aligned} \tag{6}$$

and $M$ is number of subregions in the $z$-direction. Two large numbers of $\alpha_1$ and $\alpha_2$ enforce the displacement and stress continuity, respectively. However, $\alpha_2$ must be selected carefully to avoid the excessive continuity for stresses. Because of the mixed formulation for the stress and the displacements, erroneous results in stress may ruin the ones in displacement, and vice versa. The effect of the penalty parameters will be discussed later.

Because of the complexity of the modified variational equation, it is more desirable to obtain the solution numerically rather than analytically. Rayleigh–Ritz approximation can yield a system of linear equations that is solvable numerically. As mentioned in part I, there are two possible approaches, finite element or finite difference, which can be taken to solve the system of equations numerically, and the former is taken in this study.

Because of the through-the-thickness ($z$) integration during formulation, the mixed variational equation, Eq. (5), is only a function of $x$ and $y$, so are the $29N_s$ unknown variables ($C_i^{(k)}(x,y),\ i = 1,\ldots,29$) for the $k$th subregion, where $N_s$ is the number of subregions. Among 29 unknown variables for each subregion, 16 are for the stress components, and 13 are for the displacement components, as in Eq. (8). The variational equation is then discretized in $x$- and $y$-directions for the finite element formulation. The unknown variables is collected in a vector,

$$\left\{ C_i^{(k)}(x,y) \right\} = \begin{Bmatrix} \mathbf{p}^{(k)} \\ \mathbf{d}^{(k)} \end{Bmatrix} \tag{7}$$

where

$$\begin{aligned} \mathbf{p}^{(k)} &= \{p_{11}, p_{12}, p_{21}, p_{22}, p_{31}, p_{32}, p_{33}, p_{34}, p_{41}, p_{42}, p_{43}, p_{51}, p_{52}, p_{53}, p_{61}, p_{62}\}^{(k)\mathrm{T}} \\ \mathbf{d}^{(k)} &= \{\bar{u}, u^*, u_1, u_2, \bar{v}, v^*, v_1, v_2, \bar{w}, w^*, \hat{w}, w_1, w_2\}^{(k)\mathrm{T}} \end{aligned} \tag{8}$$

Each of the unknown variables, $C_i^{(k)}(x,y)$, are then interpolated with their nodal contribution, $C_{ij}^{(k)}$, by shape functions, as follows:

$$\begin{aligned} p_i^{(k)}(x,y) &= \sum_{j=1}^{N_{\mathrm{en}}} p_{ij}^{(k)} N_{\mathrm{pj}}(x,y) \\ d_i^{(k)}(x,y) &= \sum_{j=1}^{N_{\mathrm{en}}} d_{ij}^{(k)} N_{\mathrm{dj}}(x,y) \end{aligned} \tag{9}$$

where $N_{\mathrm{en}}$ is the number of nodal points in an element, and $N_{\mathrm{pj}}$ and $N_{\mathrm{dj}}$ are the shape functions for the stress and displacement degree of freedoms, respectively. The shape functions can be chosen as linear polynomial for four-node quadrilateral elements ($N_{\mathrm{en}} = 4$), quadratic polynomial for eight-node serendipity elements ($N_{\mathrm{en}} = 8$), and etc.

The nodal values of the unknown variables for each finite element are collected in a vector,

$$\mathbf{C}^{(k)}(x,y) = \left\{ C_{ij}^{(k)} \right\} = \left\{ \mathbf{p_1}, \mathbf{d_1}, \mathbf{p_2}, \mathbf{d_2}, \ldots, \mathbf{p}_j, \mathbf{d}_j, \ldots, \mathbf{p}_{N_{\mathrm{en}}}, \mathbf{d}_{N_{\mathrm{en}}} \right\}^{(k)\mathrm{T}} \tag{10}$$

where

$$\begin{aligned}\mathbf{p}_j &= \{p_{11}, p_{12}, p_{21}, p_{22}, p_{31}, p_{32}, p_{33}, p_{34}, p_{41}, p_{42}, p_{43}, p_{51}, p_{52}, p_{53}, p_{61}, p_{62}\}_j^{\mathrm{T}} \\ \mathbf{d}_j &= \left\{\bar{u}, u^*, u_1, u_2, \bar{v}, v^*, v_1, v_2, \bar{w}, w^*, \hat{w}, w_1, w_2\right\}_j^{\mathrm{T}}\end{aligned} \tag{11}$$

The Rayleigh–Ritz approximation yields a system of linear equations by taking derivatives of the variational energy equation with respect to the independent unknown variables as follows:

$$\frac{\partial J^{(k)}}{\partial C_{ij}^{(k)}} = 0 \tag{12}$$

The system of equations is then expressed in the matrix form,

$$\begin{bmatrix} \mathbf{A} & \mathbf{C} \\ \mathbf{C}^{\mathrm{T}} & \mathbf{0} \end{bmatrix}^{(k)} \begin{Bmatrix} \mathbf{p} \\ \mathbf{d} \end{Bmatrix}^{(k)} = \begin{Bmatrix} \mathbf{f_1} \\ \mathbf{f_2} \end{Bmatrix}^{(k)} \tag{13}$$

with

$$\begin{aligned}\mathbf{A} &= \int_{\Omega} \mathbf{N}_{\boldsymbol{p}}^{\mathrm{T}} \mathbf{S} \mathbf{N}_{\boldsymbol{p}} \, \mathrm{d}\Omega \\ \mathbf{C} &= \int_{\Omega} \mathbf{N}_{\boldsymbol{p}}^{\mathrm{T}} \mathbf{B} \mathbf{N}_{\boldsymbol{d}} \, \mathrm{d}\Omega \\ \mathbf{f_1} &= \mathbf{0} \\ \mathbf{f_2} &= \int_{\Gamma_\sigma} \mathbf{N}_{\boldsymbol{d}}^{\mathrm{T}} \tilde{\boldsymbol{\tau}} \, \mathrm{d}\Gamma\end{aligned} \tag{14}$$

where $\mathbf{S}$, $\mathbf{B}$, $\mathbf{N}_{\boldsymbol{p}}$ and $\mathbf{N}_{\boldsymbol{d}}$ are matrices for the compliance, relationship between the stresses and displacements, and the shape functions for the stress and displacement degree of freedoms, respectively.

The equations for the constraint conditions at the interface are also obtained by

$$\frac{\partial J_{\mathrm{c}}^{(k)}}{\partial C_{ij}^{(k)}} = 0 \quad \text{and} \quad \frac{\partial J_{\mathrm{c}}^{(k)}}{\partial C_{ij}^{(l)}} = 0 \tag{15}$$

which yield the matrix form,

$$\begin{bmatrix} \mathbf{Q}_{\boldsymbol{P}} & \mathbf{0} & -\mathbf{Q}_{\boldsymbol{P}} & \mathbf{0} \\ \mathbf{0} & \mathbf{Q}_{\boldsymbol{d}} & \mathbf{0} & -\mathbf{Q}_{\boldsymbol{d}} \\ -\mathbf{Q}_{\boldsymbol{P}}^{\mathrm{T}} & \mathbf{0} & \mathbf{Q}_{\boldsymbol{P}} & \mathbf{0} \\ \mathbf{0} & -\mathbf{Q}_{\boldsymbol{d}}^{\mathrm{T}} & \mathbf{0} & \mathbf{Q}_{\boldsymbol{d}} \end{bmatrix} \begin{Bmatrix} \mathbf{p}^{(k)} \\ \mathbf{d}^{(k)} \\ \mathbf{p}^{(l)} \\ \mathbf{d}^{(l)} \end{Bmatrix} = \mathbf{0} \tag{16}$$

with

$$\begin{aligned}\mathbf{Q}_{\boldsymbol{d}} &= \alpha_1 \int_{\Omega} \mathbf{N}_{\boldsymbol{d}}^{\mathrm{T}} \mathbf{N}_{\boldsymbol{d}} \, \mathrm{d}\Omega \\ \mathbf{Q}_{\boldsymbol{P}} &= \alpha_2 \int_{\Omega} \mathbf{N}_{\boldsymbol{p}}^{\mathrm{T}} \mathbf{h}_{,x} \mathbf{N}_{\boldsymbol{p}} \, \mathrm{d}\Omega\end{aligned} \tag{17}$$

where $\mathbf{h}_{,x}$ is a matrix containing the slopes of the interfacial surfaces in $x$- and $y$-directions as in Eq. (4). The global system of equations is then formulated by combining the elemental stiffness matrix and force vectors in Eqs. (13) and (16), and solved numerically to obtain the displacement and stress results.

## 3. Results

The present mixed finite element method is applied to flat laminated composites and a RVE of woven composites. Results are compared with previous works and/or those given by displacement-based finite element method.

### 3.1. Flat laminated composites

We solved a class of boundary value problems known as the free edge problem in which a flat laminate of finite width is subject to a uniform axial displacement ($\bar{u}$). The origin of coordinates is located at the center of the laminate and the laminate is symmetric ($\theta(z) = \theta(-z)$). Each layer is treated as a transversely isotropic material with a layup of $[0/90]_s$, where 0° is parallel with the $x$-axis, as in Fig. 2. The layers are of equal thickness, $h$, and the laminate width is $2b = 16h$. The material properties are listed in Table 1.

The following boundary conditions are applied to simulate a tensile loading subject to a uniform displacement in the $x$-direction. The axial displacement in $x$-direction at $x = 0$ ($yz$-surface) is fixed, and at $x = L_x$ is prescribed with $\bar{u}$. Symmetric boundary condition is enforced at $y = 0$ ($xz$-surface) by setting $v = 0$. The zero vertical displacement at $z = 0$ simulates a case where laminates are symmetrically stacked.

$$\begin{aligned}
&u_1^{(k)}(0,y,z) = u_2^{(k)}(0,y,z) = 0, \qquad \bar{u}^{(k)}(0,y,z) = u^{*(k)}(0,y,z) = 0\\
&u_1^{(k)}(L_x,y,z) = u_2^{(k)}(L_x,y,z) = \bar{u}, \qquad \bar{u}^{(k)}(L_x,y,z) = u^{*(k)}(L_x,y,z) = \frac{\bar{u}}{2}\\
&v_1^{(k)}(x,0,z) = v_2^{(k)}(x,0,z) = 0, \qquad \bar{v}^{(k)}(x,0,z) = v^{*(k)}(x,0,z) = 0\\
&w_1^{(k)}(x,y,0) = 0
\end{aligned} \tag{18}$$

The penalty parameters in Eq. (6) are chosen as $\alpha_1 = 10^3$ and $\alpha_2 = 10^2$ to avoid numerical instability. Two different meshes are generated for the present mixed method: Having the same number of divisions in

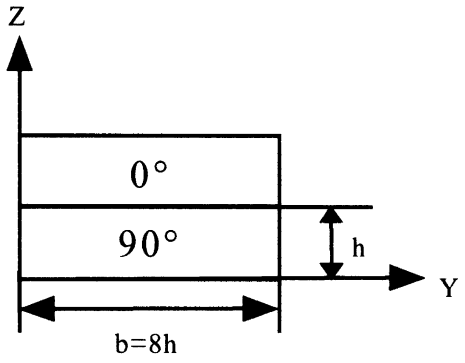


Fig. 2. Flat laminated composites.

Table 1
Material properties of [T300/N5208]

| $E_x$ (GPa) | $E_y$ (GPa) | $E_z$ (GPa) | $v_{xy}$ | $v_{xz}$ | $v_{yz}$ | $G_{xy}$ (GPa) | $G_{xz}$ (GPa) | $G_{yz}$ (GPa) |
|---|---|---|---|---|---|---|---|---|
| 181 | 10.3 | 10.3 | 0.28 | 0.28 | 0.5 | 7.17 | 7.17 | 7.05 |

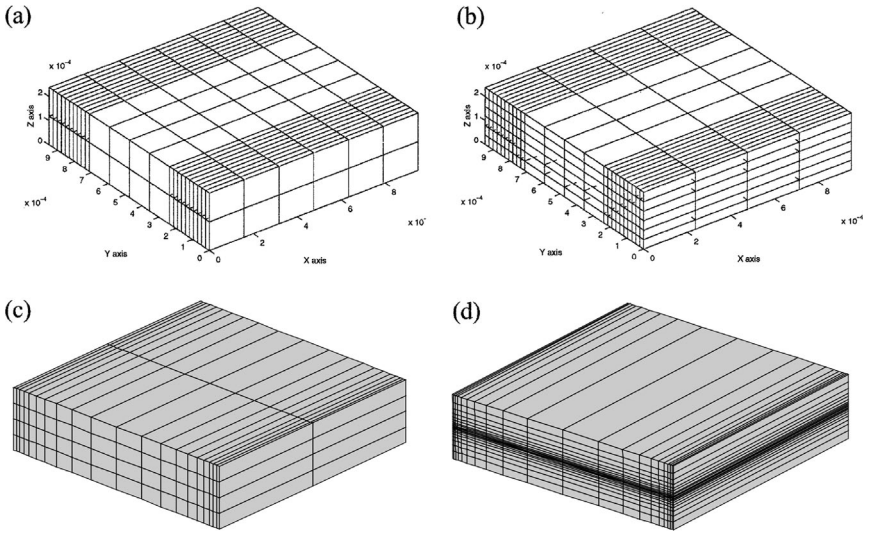


Fig. 3. Geometry and number of divisions for present mixed and displacement-based finite element methods. (a) mixed ($N_x = 6$, $N_y = 24, N_z = 1$); (b) mixed ($N_x = 4, N_y = 24, N_z = 3$); (c) FEM ($N_x = 2, N_y = 20, N_z = 2$); (d) FEM ($N_x = 1, N_y = 20, N_z = 10$).

the $y$-axis, one has only one sublayer, and the other has three sublayers in each ply (subregion) in the $z$-axis. The number of divisions and mesh are shown in Fig. 3(a) and (b).

Stress and displacement results are compared with the finite element method and a previous work by Pagano (1978). For the finite element method, three-dimensional eight-node brick elements are used with two different meshes; one has two divisions, and the other has 10 divisions in the $z$-direction in each subregion, as in Fig. 3(c) and (d). The interfacial stresses are calculated by interpolating the elemental stresses at the Gaussian integration points into the nodal points along the interface. Thus, two normal and shear stresses are calculated by interpolating those of the upper and the lower elements at the interface. In the meanwhile, two-dimensional mixed analysis is done by Pagano (1978) with 18 sublayers.

Fig. 4 shows the results of the present method (mixed) compared with those of the FEM and Pagano. The results show that the normal and shear stresses become singular at the free edge ($y = L_y$) because of the discontinuity in the elastic properties. The present and Pagano's methods, which are both the mixed methods, yield nearly identical results for the transverse displacement at the top surface (Fig. 4(a)), the normal stress along the [0/90] interface (Fig. 4(b)), and the normal stress along the central surface (Fig. 4(d)), whereas the displacement-based FEM shows little difference with them. The FEM does not yield an accurate solution without a sufficient number of sublayers in the $z$-direction, whereas the present method shows an excellent agreement even with one layer except at a region close to the free edge.

While Pagano's solution yields zero shear stress with a high peak at the free edge ($y = L_y$), the present and FEM solutions give finite values, as Fig. 4(c) shows. This is because the linear shape functions used in both finite element methods are not accurate enough to capture the drastic stress change at the free edge. Although the increment of the sublayer in the present mixed method makes the peak value higher, it creates wiggles in the shear–stress distribution near the free edge. This is because the high stress gradient at the free edge influences on the stress field inside the edge. As pointed out earlier, the excessive continuity for stresses should be avoided at singularities and at abrupt material property change interfaces. Therefore, the penalty method is more suitable than the irreducible formulation because it can relieve the excessiveness by controlling the penalty parameter for the stress constraint condition ($\alpha_2$). Note that, in this case of such an extremely high stress gradient, even the penalty method cannot cure the problem completely.

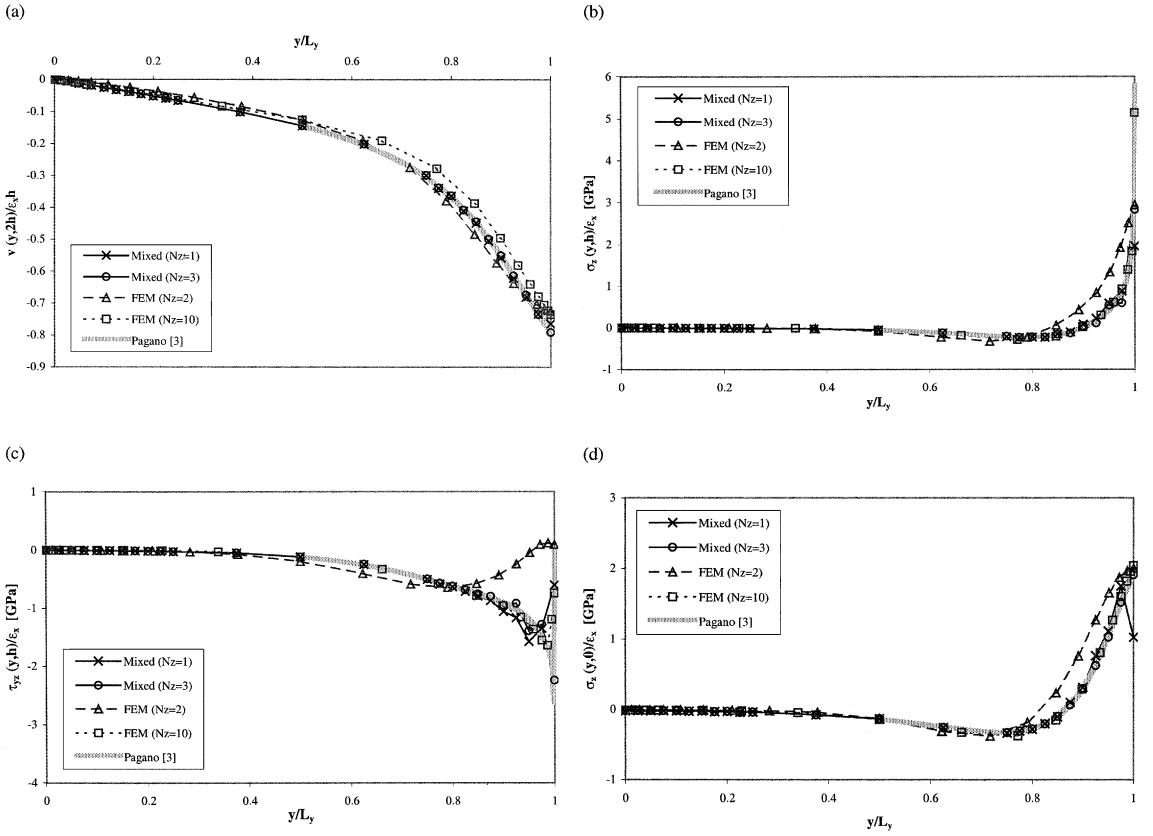


Fig. 4. Stress and displacement results for flat laminated composites. (a) Transverse displacement at top surface ($z = 2h$); (b) distribution of $\sigma_z$ along [0/90] interface ($z = h$); (c) distribution of $\tau_{yz}$ along [0/90] interface ($z = h$); (d) distribution of $\sigma_z$ along central plane ($z = 0$).

The normal stress at the central surface (Fig. 4(d)) with one sublayer shows a good agreement with Pagano's solution except a hump at the free edge. This hump does not appear with three sublayer solutions.

### 3.2. Representative volume element of woven-fabric composites

The RVE of the model is divided into several subregions; each subregion is occupied by a characteristic fabric yarn or a matrix (see Fig. 5). $L_x$ and $L_y$ are the length of RVE in the $x$- (warp) and $y$- (fill) directions, and $t_w$ and $t_f$ half of the thickness of the warp and fill yarn, respectively. The yarn is assumed as transversely isotropic, and the matrix as isotropic materials. Each yarn and the matrix subregion of the RVE are discretized into several finite elements in the longitudinal and transverse directions. $N_x$ and $N_y$ are the numbers of subdivisions in half of the length of RVE in the $x$- and the $y$-directions ($L_x/2$ and $L_y/2$) respectively.

The cross-sectional boundary of the yarn is confined by $h_L = h_1$ (lower boundary) and $h_U = h_2$ (upper boundary). Because of yarn waviness and elliptical cross-sectional boundary of the yarns, $h_L$ and $h_U$ are functions of both $x$ and $y$. Yarn waviness at each subregion is assumed to be sinusoidal functions. Lower and upper surface coordinates of the yarn subregions are as follows:

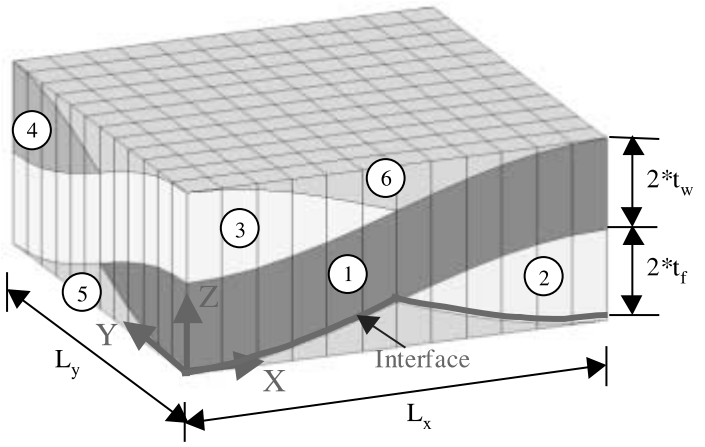


Fig. 5. RVE of a plain-woven composites. Numbers in circles indicate the numbers of subregions.

$$
\begin{aligned}
h_{\mathrm{L}}^{(1)} &= t_{\mathrm{f}}\left(1-\cos\frac{\pi x}{L_x}\right)+t_{\mathrm{w}}\left(1-\cos\frac{\pi y}{L_y}\right), \quad h_{\mathrm{U}}^{(1)} = t_{\mathrm{f}}\left(1-\cos\frac{\pi x}{L_x}\right)+t_{\mathrm{w}}\left(1+\cos\frac{\pi y}{L_y}\right)\\
h_{\mathrm{L}}^{(2)} &= t_{\mathrm{f}}\left(1+\cos\frac{\pi x}{L_x}\right)+t_{\mathrm{w}}\left(1-\cos\frac{\pi y}{L_y}\right), \quad h_{\mathrm{U}}^{(2)} = t_{\mathrm{f}}\left(1-\cos\frac{\pi x}{L_x}\right)+t_{\mathrm{w}}\left(1-\cos\frac{\pi y}{L_y}\right)\\
h_{\mathrm{L}}^{(3)} &= t_{\mathrm{f}}\left(1-\cos\frac{\pi x}{L_x}\right)+t_{\mathrm{w}}\left(1+\cos\frac{\pi y}{L_y}\right), \quad h_{\mathrm{U}}^{(3)} = t_{\mathrm{f}}\left(1+\cos\frac{\pi x}{L_x}\right)+t_{\mathrm{w}}\left(1+\cos\frac{\pi y}{L_y}\right)\\
h_{\mathrm{L}}^{(4)} &= t_{\mathrm{f}}\left(1+\cos\frac{\pi x}{L_x}\right)+t_{\mathrm{w}}\left(1+\cos\frac{\pi y}{L_y}\right), \quad h_{\mathrm{U}}^{(4)} = t_{\mathrm{f}}\left(1+\cos\frac{\pi x}{L_x}\right)+t_{\mathrm{w}}\left(1-\cos\frac{\pi y}{L_y}\right)
\end{aligned}
\tag{19}
$$

where superscript indicates the subregion number. Lower and upper surface coordinates of the bottom and top matrix subregions are as follows:

$h_{\mathrm{L}}^{(5)} = 0$, and

$$
h_{\mathrm{U}}^{(5)} = \begin{cases}
t_{\mathrm{f}}(1-\cos\frac{\pi x}{L_x})+t_{\mathrm{w}}(1-\cos\frac{\pi y}{L_y}) & \text{for } 0\leqslant x\leqslant L_x/2, 0\leqslant y\leqslant L_y/2\\
t_{\mathrm{f}}(1+\cos\frac{\pi x}{L_x})+t_{\mathrm{w}}(1-\cos\frac{\pi y}{L_y}) & \text{for } L_x/2\leqslant x\leqslant L_x, 0\leqslant y\leqslant L_y/2\\
t_{\mathrm{f}}(1-\cos\frac{\pi x}{L_x})+t_{\mathrm{w}}(1+\cos\frac{\pi y}{L_y}) & \text{for } 0\leqslant x\leqslant L_x/2, L_y/2\leqslant y\leqslant L_y\\
t_{\mathrm{f}}(1+\cos\frac{\pi x}{L_x})+t_{\mathrm{w}}(1+\cos\frac{\pi y}{L_y}) & \text{for } L_x/2\leqslant x\leqslant L_x, L_y/2\leqslant y\leqslant L_y
\end{cases}
\tag{20}
$$

$$
h_{\mathrm{L}}^{(6)} = \begin{cases}
t_{\mathrm{f}}(1+\cos\frac{\pi x}{L_x})+t_{\mathrm{w}}(1+\cos\frac{\pi y}{L_y}) & \text{for } 0\leqslant x\leqslant L_x/2, 0\leqslant y\leqslant L_y/2\\
t_{\mathrm{f}}(1-\cos\frac{\pi x}{L_x})+t_{\mathrm{w}}(1+\cos\frac{\pi y}{L_y}) & \text{for } L_x/2\leqslant x\leqslant L_x, 0\leqslant y\leqslant L_y/2\\
t_{\mathrm{f}}(1+\cos\frac{\pi x}{L_x})+t_{\mathrm{w}}(1-\cos\frac{\pi y}{L_y}) & \text{for } 0\leqslant x\leqslant L_x/2, L_y/2\leqslant y\leqslant L_y\\
t_{\mathrm{f}}(1-\cos\frac{\pi x}{L_x})+t_{\mathrm{w}}(1-\cos\frac{\pi y}{L_y}) & \text{for } L_x/2\leqslant x\leqslant L_x, L_y/2\leqslant y\leqslant L_y
\end{cases}
\tag{21}
$$

and $h_{\mathrm{U}}^{(6)} = 2(t_{\mathrm{f}}+t_{\mathrm{w}})$.

The following boundary conditions are prescribed to simulate a tensile loading subject to a uniform displacement in the $x$-direction with lateral constraint in the $y$-direction. The zero vertical displacement at $z = 0$ simulates a case where two RVEs are symmetrically stacked.

$$
\begin{aligned}
&u_1^{(k)}(0,y,z) = u_2^{(k)}(0,y,z) = 0, \quad \bar{u}^{(k)}(0,y,z) = u^{*(k)}(0,y,z) = 0 \\
&u_1^{(k)}(L_x,y,z) = u_2^{(k)}(L_x,y,z) = \bar{u}, \quad \bar{u}^{(k)}(L_x,y,z) = u^{*(k)}(L_x,y,z) = \frac{\bar{u}}{2} \\
&v_1^{(k)}(x,0,z) = v_2^{(k)}(x,0,z) = v_1^{(k)}(x,L_y,z) = v_2^{(k)}(x,L_y,z) = 0 \\
&\bar{v}^{(k)}(x,0,z) = v^{*(k)}(x,0,z) = \bar{v}^{(k)}(x,L_y,z) = v^{*(k)}(x,L_y,z) = 0 \\
&w_1^{(k)}(x,y,0) = 0
\end{aligned}
\tag{22}
$$

Fig. 6(a) shows deformed shape under the above boundary conditions. The top surface of the RVE is twisted because of its anti-symmetric geometry in the $x$- and $y$-directions. Fig. 6(b) shows the anti-symmetric distributions of the vertical displacement at the intersection of the top surface and the $xz$-planes at $y = 0$ and $y = L_y$.The thickness of the matrix subregions (subregions 5 and 6) at four corner points is zero according to the model. Physically, the lower $(w_1)$ and upper $(w_2)$ vertical displacements at these corners should be the same. However, because of the numerical errors, they do not match with each other with the coarse meshes $(N_x < 3)$, as in Fig. 6(c). Therefore, finer meshes $(N_x \geqslant 4)$ should be used to achieve the interface continuity, and $N_x = 6$ is chosen in this study.

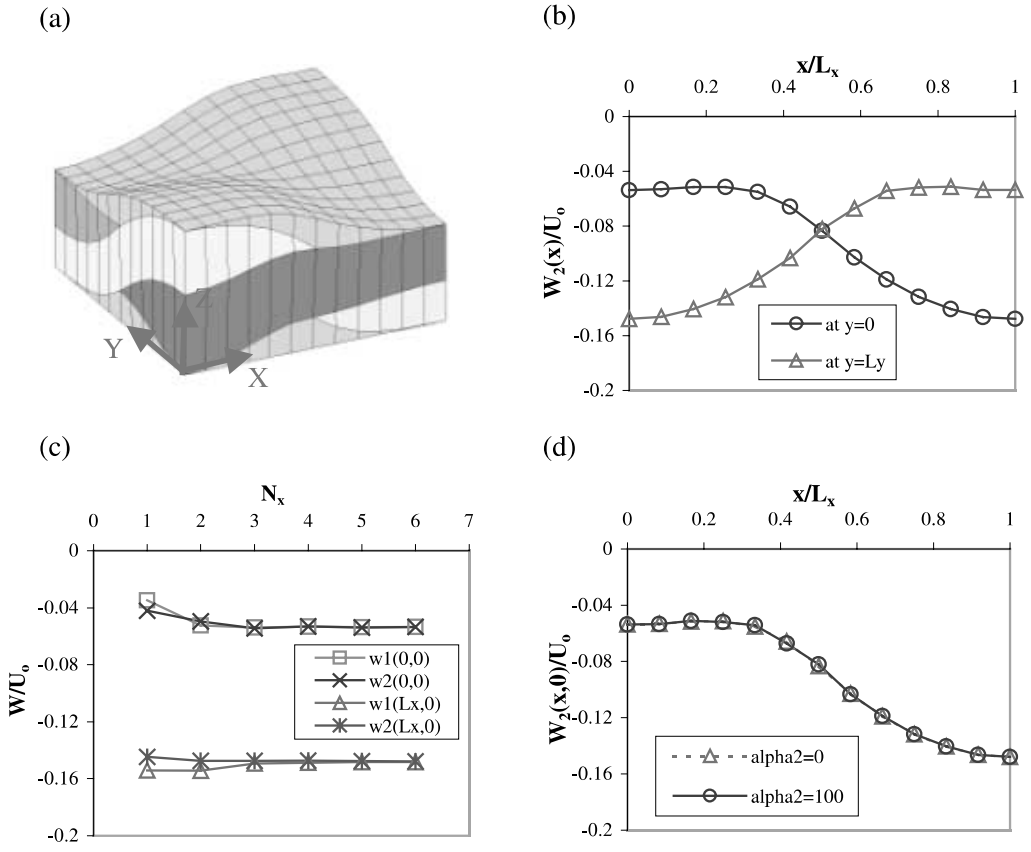


Fig. 6. Displacement results of RVE of woven composites. (a) deformed shape $(N_x = 6)$; (b) vertical displacements at top surface; (c) convergence of model $(\alpha_2 = 100)$; (d) vertical displacements with two $\alpha_2$.

While one displacement penalty parameter is set as $\alpha_1 = 10^3$, two stress penalty parameters are chosen as $\alpha_2 = 10^2$ and $\alpha_2 = 0$ for a sensitivity study. The latter case ($\alpha_2 = 0$) means no stress constraint condition is enforced. Fig. 6(d) shows that the vertical displacement distributions are almost identical with two different $\alpha_2$, which indicates that the stress continuity condition has a negligible influence on the displacement results.

Figs. 7 and 8 show in-plane and out-of-plane global stress distributions on the warp and fill yarns, respectively. Fig. 5 shows that the transverse fill yarns taper to zero thickness in the middle of the warp yarns ($x = L_x/2$), so that more matrix material with low moduli fills this region. In particular, the matrix material fills the thickness most in the vicinity of cross-yarn crimping location at $x = L_x/2$ and $y = L_y/2$, where both the warp and the fill yarns taper to zero thickness. Therefore, higher in-plane longitudinal stress ($\sigma_x$) is carried in this yarn-crimping region, and the stress concentration of $\sigma_x$ is maximum at the location of the cross-yarn crimp, as shown in Figs. 7(a) and 8(a). In-plane transverse stress ($\sigma_y$) is concentrated at the cross-yarn crimping region for the same reason.

Figs. 7(c), (d) and 8(c), (d) show out-of-plane normal and shear–stress distributions. These stresses are evaluated in the global coordinate system. The positive out-of-plane normal stress ($\sigma_z$) as the potential delaminating stress occurs at corners where the deformed warp yarns concave upward for this loading condition and symmetric stacking of the RVEs. As Fig. 7(d) shows, the out-of-plane shear stress ($\tau_{xz}$) is maximum at the midlength of the warp yarns where the crimping angle is maximum, and changes the sign with the crimping direction.

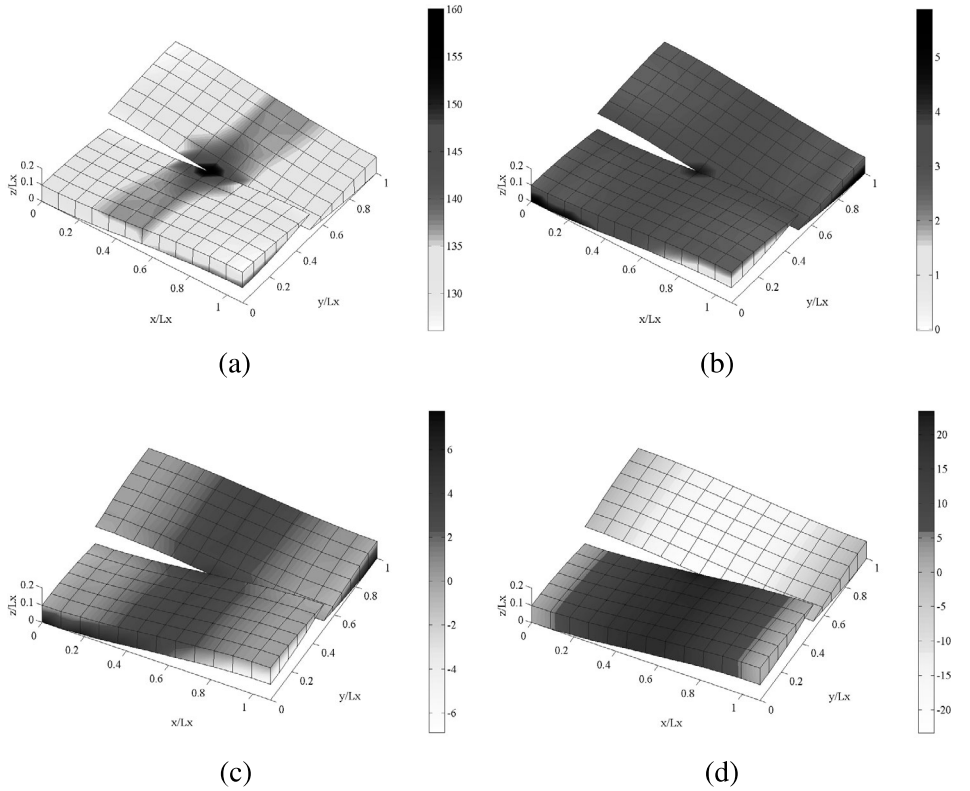


Fig. 7. Stress distribution on longitudinal warp yarns of the RVE (subregions 1 and 4). (a) $\sigma_x/\varepsilon_x$ (GPa); (b) $\sigma_y/\varepsilon_x$ (GPa); (c) $\sigma_z/\varepsilon_x$ (GPa); (d) $\tau_{xz}/\varepsilon_x$ (GPa).

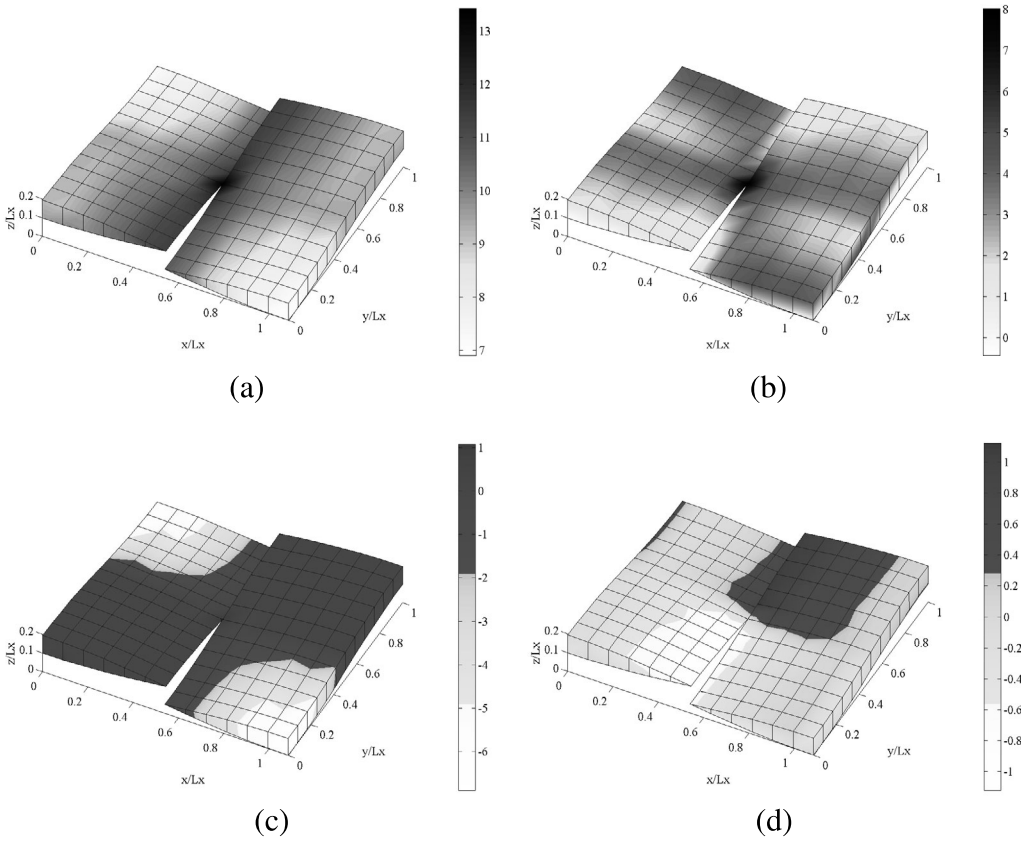


Fig. 8. Stress distribution on transverse fill yarns of the RVE (subregions 2 and 3). (a) $\sigma_x/\varepsilon_x$ (GPa); (b) $\sigma_y/\varepsilon_x$ (GPa); (c) $\sigma_z/\varepsilon_x$ (GPa); (d) $\tau_{xz}/\varepsilon_x$ (GPa).

Fig. 9 shows the normal and shear–stress distributions along an interfacial line in Fig. 3. These interfacial stresses are the local ones in Eq. (4), which are transformed from the stress components in the global coordinate system by the slopes of the interfacial surfaces. The subscript ($k$) indicates the bottom matrix subregion (subregion 5), and ($l$) indicates the upper yarns lying on top of the matrix (i.e., subregion 1 at $0 \leqslant x \leqslant L_x/2$ and subregion 3 at $L_x/2 \leqslant x \leqslant L_x$). Fig. 9(a) and (d) show that the interfacial normal stresses from the lower and the upper subregion agrees well with each other with only one sublayer in the thickness ($z$) direction. The normal stress continuity can be achieved well even without the stress constraint condition ($\alpha_2 = 0$). It also shows a smooth transition of the stress distribution with a significant change in the material properties at $x = L_x/2$.

Fig. 9(c)–(f) show that the interfacial shear–stress continuity is achieved fairly well with the present method, except the region near $x = L_x/2$, where the high stress gradient is observed. The reason of the high stress gradient in the local shear stresses is that the local shear stresses ($\hat{\sigma}_4$ and $\hat{\sigma}_5$) are highly affected by the global axial stresses ($\sigma_1$ and $\sigma_2$) as in Eq. (4), and these axial stresses change abruptly with the change in the material properties at this region. The interfacial shear stresses do not match well at this region because the thickness of the subregion 3 is zero at $x = L_x/2$. While two subregions (subregions 5 and 1) are considered in calculating the interfacial stresses at the left-hand side of $x = L_x/2$, three subregions (subregions 5, 3 and 1) are considered in the calculation at the right-hand side because of the zero thickness of the subregion 3. Therefore, the stress continuity condition becomes,

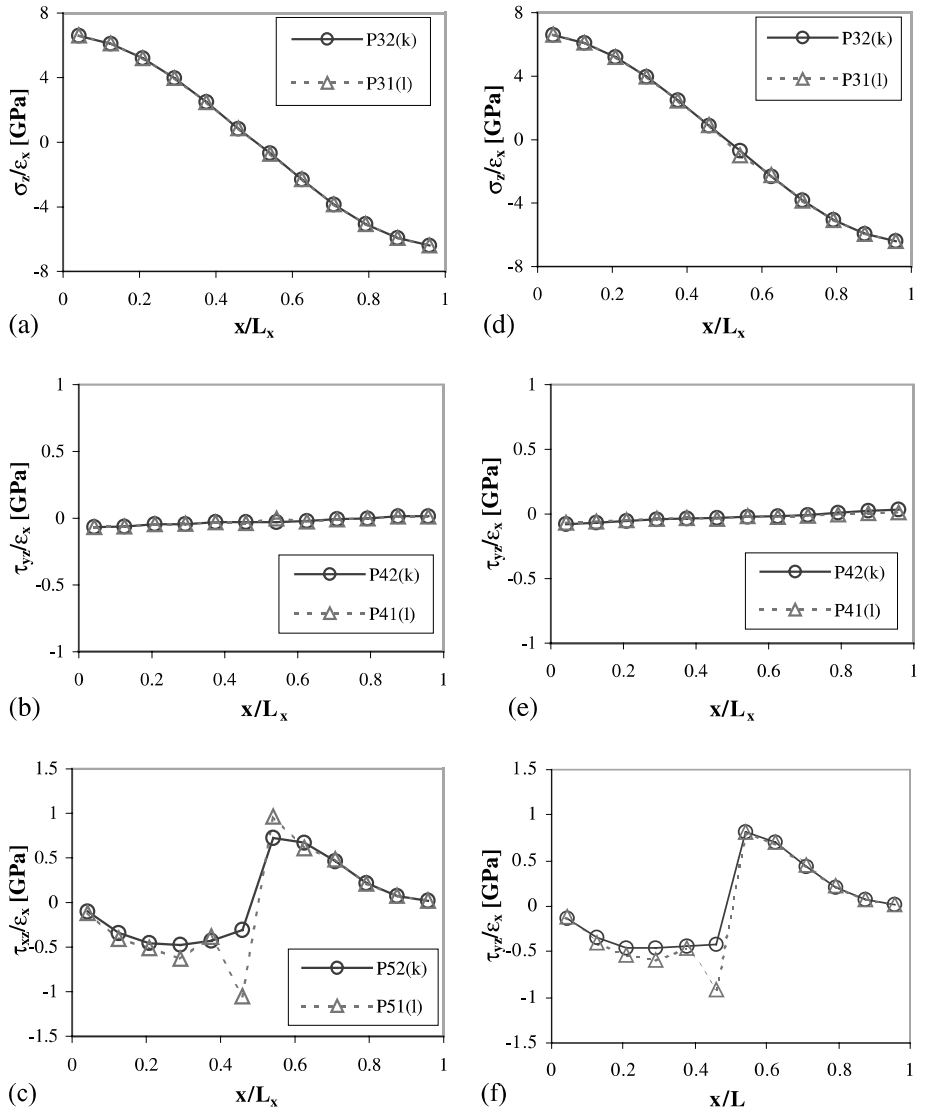


Fig. 9. Interfacial normal and shear–stress distributions of RVE of woven composites with two different penalty parameters for stress continuity condition. (a) normal stress ($\sigma_z$) with $\alpha_2 = 100$; (b) shear stress ($\tau_{yz}$) with $\alpha_2 = 100$; (c) shear stress ($\tau_{xz}$) with $\alpha_2 = 100$; (d) normal stress ($\sigma_z$) with $\alpha_2 = 0$; (e) shear stress ($\tau_{yz}$) with $\alpha_2 = 0$; (f) shear stress ($\tau_{xz}$) with $\alpha_2 = 0$.

(1) at left-hand side of $x = L_x/2$,

$$\hat{P}_{42}^{(5)} = \hat{P}_{41}^{(1)} \quad \text{and} \quad \hat{P}_{52}^{(5)} = \hat{P}_{51}^{(1)} \tag{23}$$

(2) at right-hand side of $x = L_x/2$,

$$\hat{P}_{42}^{(5)} = \hat{P}_{41}^{(3)} = \hat{P}_{42}^{(3)} = \hat{P}_{41}^{(1)} \quad \text{and} \quad \hat{P}_{52}^{(5)} = \hat{P}_{51}^{(3)} = \hat{P}_{52}^{(3)} = \hat{P}_{51}^{(1)} \tag{24}$$

where $\hat{P}_i^{(k)}$ is the local component of the interfacial stresses at the $k$th subregion. However, it is hard to satisfy such a continuity condition with the zero thickness because of the numerical error in evaluating the

stress components. The numerical error in the axial stresses, whose magnitudes are much larger than those of the shear stresses, affects the interfacial shear stresses significantly, so that jumps and mismatches are observed at this region.

Fig. 9(b)–(f) also show that the shear stress distribution is smoother without the stress constraint condition ($\alpha_2 = 0$) than $\alpha_2 = 100$. As observed in the flat laminated case, the excessive stress continuity conditions are not necessary in the present mixed method, and should be avoided at the stress singularity or the material mismatch. Not shown on the figure are the results for $\alpha_2 \gg \alpha_1$, which make a little improvement in the stress continuity, but cause the displacement results unrealistic and far different from the one in Fig. 6(a).

## 4. Conclusions

Three-dimensional displacements and stresses are analyzed numerically based on the Reissner's mixed variational principle and derived by Roy and Sihn in part I of this work. The three-dimensional model is treated semi two-dimensionally by making an assumption on the interlaminar stress variations, and integrating the variational energy in the thickness direction. Additional energy terms are added to the variational energy to impose the displacement and stress continuity at the interface by the penalty approach. Two penalty parameters are employed to enforce the displacement and the stress continuity condition, respectively. The Rayleigh–Ritz approximation with polynomial shape functions yields a system of linear equations by taking derivatives of the variational energy equation with respect to the independent unknown variables.

The present method is applied to analyze flat laminated composites with a free edge and the RVE of the plain-woven composites. The results are compared and validated with the displacement-based finite element analysis and/or analytic solution. Since the stresses are evaluated pointwise without any interpolation of the displacement results, more accurate interlaminar stresses are obtained at the interfaces between two different materials with a few number of sublayers compared with the displacement-based finite element analysis.

The interfacial normal and shear–stress continuity is achieved well with the penalty approach except the region where the thickness of the subregions is small. It is found that the imposition of the displacement continuity condition is more important than that of the stress continuity condition. Furthermore, the excessive continuity condition in the stress fields is not necessary, and may induce convergence instability in the data of the displacement as well as the stress fields. Imposing only the displacement constraint without the stress constraint yields a smoother interfacial normal and shear–stress distribution than the case considering both constraint conditions.

## References

Harrison, P.E., Johnson, E.R., 1996. A mixed variational formulation for interlaminar stresses in thickness-tapered composite laminates. International Journal of Solids and Structures 33 (16), 2377–2399.

Pagano, N.J., 1978. Stress fields in composite laminates. International Journal of Solids and Structures 14, 385–400.

Reissner, E., 1950. On a variational theorem in elasticity. Journal of Mathematics and Physics 29, 90–95.

Roy, A.K., Sihn, S., 2000. Development of a three-dimensional mixed variational model for woven composites: part I – mathematical formulation. International Journal of Solids and Structures 38, 5935–5947.

Zienkiewicz, O.C., Taylor, R.L., 1988. The finite element method, fourth edition, vol. 1. McGraw-Hill, New York.